Catalysis Science & Technology

ROYAL SOCIETY OF CHEMISTRY

PAPER

View Article Online
View Journal

Cite this: DOI: 10.1039/d4cy00765d

Effect of pretreatment conditions on Fe-ZSM-5 properties and performance for Fischer–Tropsch synthesis†

Jane N. Agwara, [a] Denis Leshchev, [b] Sinhara M. H. D. Perera, [a] Alexis K. Bauer, [c] Michael L. Neidig [c] and Marc D. Porosoff *[a]

Received 19th June 2024,
Accepted 18th November 2024

DOI: 10.1039/d4cy00765d

rsc.li/catalysis

Iron supported on ZSM-5 is a widely studied catalyst for Fischer–Tropsch synthesis (FTS). Iron is activated with H_2, CO, or a mixture of CO and H_2 prior to FTS, resulting in phase transformations that make it challenging to understand structure–property relationships. In this work, we demonstrate that increasing the pretreatment temperature of Fe–Na-ZSM-5 reduces CO conversion irrespective of the reductant, but the product selectivity, iron particle size, composition, CO adsorption properties, and zeolite structure is dependent on both the pretreatment temperature and reductant. Pretreatment of Fe–Na-ZSM-5 in H_2 induces sintering of iron particles, increasing C_2–C_4 olefins and C_{5+} hydrocarbons selectivity from 19.0% and 14.0% at 350 °C to 28.2% and 25.4% at 770 °C, respectively. Conversely, CO pretreatment facilitates carbide formation, coke deposition, and CH_4 formation.

1. Introduction

Iron-based catalysts are widely used for the conversion of carbon monoxide (CO) to hydrocarbons *via* Fischer–Tropsch synthesis (FTS), offering advantages such as high activity, hydrocarbon selectivity, limited methane (CH_4) selectivity, and improved water-gas shift activity compared to other active FTS metals like cobalt.[1–3] Iron-based catalysts are often pretreated with hydrogen (H_2), CO, or a CO–H_2 mixture at temperatures ranging from 250 to 800 °C to activate the catalyst, leading to the formation of iron oxides and/or carbides with the desired performance.[4–6] Bian *et al.*[7] studied precipitated iron oxides (Fe_2O_3) and reported that the surface area of CO-pretreated Fe_2O_3 remained similar to the as-synthesized catalyst, but the surface area of the H_2-pretreated sample was five times lower, potentially due to sintering. Ding *et al.*[8] observed that H_2-pretreated iron supported on silica (Fe–Mn–K–SiO_2) exhibited a higher surface area than CO or CO–H_2 pretreated catalysts, possibly attributed to pore blockage by carbonaceous species.

The complexity of the *in situ* transformation of iron adds to the importance of selecting appropriate pretreatment conditions, as iron undergoes conversion into combinations of metallic iron (Fe^0), iron oxides (Fe_3O_4, FeO), and/or carbides (*e.g.* Fe_5C_2, Fe_3C, Fe_7C_3) during pretreatment. Because FTS is a structure-sensitive reaction,[9,10] understanding how the pretreatment conditions affect the reactor performance is critically important.[11–14] Existing studies on the effect of pretreatment conditions on the performance of iron-based catalysts have primarily focused on precipitated iron,[7,15–20] promoted precipitated iron,[8,18,21–23] and iron supported on silica.[24–28] SBA-15 has been used because of high surface area (700–1040 $m^2\ g^{-1}$) and a narrow pore-size distribution (5–30 nm) that enables introduction of iron nanoparticles within the pores of the support, minimizing iron migration to the outer surface, and subsequent aggregation during pretreatment and reaction.[26,27,29] Similar characteristics are present in ZSM-5 zeolites, with the added benefit of tunable acidity that can be leveraged to control FTS performance.[30,31] Although ZSM-5 is an extensively studied support for iron-based catalysts, studies on the effect of pretreatment conditions on iron supported on ZSM-5 (Fe-ZSM-5) are lacking. This can be seen in Table 1, a summary of collected Fe-based catalysts and pretreatment conditions that have been studied for FTS.[7,8,15,18–27,32,33]

Understanding the effect of FTS pretreatment conditions on Fe-ZSM-5 can be challenging because when CO is used as the reductant, CO dissociation results in carbon deposition, reduction of surface area, and in turn, decreased FTS activity.[17] In contrast, pretreating Fe-ZSM-5 with H_2

[a] Department of Chemical Engineering, University of Rochester, 4405 Wegmans Hall, Rochester, NY, 14627, USA. E-mail: marc.porosoff@rochester.edu; Tel: (+1) 585 276 7401
[b] National Synchrotron Light Source II, Brookhaven National Laboratory, Upton, NY, 11973, USA
[c] Inorganic Chemistry Laboratory, Department of Chemistry, University of Oxford, South Parks Road, Oxford OX1 3QR, UK

† Electronic supplementary information (ESI) available. See DOI: https://doi.org/10.1039/d4cy00765d

Table 1 Reported studies on the effect of reduction conditions of iron-based catalysts for FTS

	Pretreatment conditions			Reaction temp.	Highest CO conversion	
Catalyst	Gas	Temp. (°C)	Time (h)	(°C)	Pretreatment gas/product	Iron phase post-pretreatment
Fe_2O_3 (ref. 7)	CO, H_2	300	6	250	CO/C_3–C_5	Fe^0, χ-Fe_5C_2, ε′-$Fe_{2.2}C$
Fe/Si/K (ref. 15)	CO, H_2–CO	270, 300	24	270	CO/C_{2+}	χ-Fe_5C_2, ε′-$Fe_{2.2}C$
Fe/Cu/K (ref. 18)	H_2, CO, H_2–CO	250–310	8, 24	250	CO/olefins and C_{5+}	Fe^0 and surface carbon
Fe/K (ref. 19)	CO, CO–H_2	350	24	270	CO–H_2/olefins and C_{5+}	Fe_5C_2
Fe/Mn/K (ref. 21)	H_2, CO, H_2–CO	250–400	4, 8	320	CO/ C_2–C_4 olefins	Fe_5C_2
Fe/Mo and Fe (ref. 22)	H_2, CO, H_2–CO	280, 350	12	280	CO/NA	Fe^0, Fe_3O_4, χ-Fe_5C_2
Fe/Mn (ref. 23)	H_2, CO, H_2–CO	275–300	24	275	CO/CO–H_2/olefins and C_{5+}	—
Fe/Mn/K/SiO_2 (ref. 8)	H_2, CO, H_2–CO	265	24	260	CO/olefins and C_{5+}	Fe_5C_2 and carbonaceous species
Fe/NS (ref. 24)	H_2, CO, H_2–CO	750	24	270	CO/C_6–C_{14}	Likely χ-Fe_5C_2 or θ-Fe_3C
Fe/K/Si/Cu (ref. 25)	H_2, CO, H_2–CO	270	24	270	CO/total hydrocarbons	Fe_3O_4, χ-Fe_5C_2, ε′-$Fe_{2.2}C$
Fe/SBA-15 (ref. 26)	H_2, H_2–CO	330, 415	0	—	H_2/total hydrocarbons	Fe_3O_4, Fe^{2+}
Fe/SBA-15 (ref. 27)	H_2, H_2–CO	430	26	430	H_2/total hydrocarbons	α-Fe, Fe^{2+}, Fe_3O_4

accelerates the growth of iron particles, diminishing active sites.[15,16,18] The pores of the zeolite can be blocked by deposited carbon during reaction or sintered iron particles. For example, Marchetti *et al.*[34] reported that pretreating iron supported on zeolite L in H_2 resulted in sintering due to iron oxide migration and agglomeration on the external surface of the zeolite.[34]

In this study, we support iron on Na-ZSM-5, denoted as Fe–Na-ZSM-5, and systematically vary the pretreatment conditions to better understand their effect on FTS performance. We use H_2 and CO as pretreatment gases in the temperature range of 300 to 770 °C to encompass the conditions that are typically used for FTS pretreatment. We find that CO conversion decreases with increasing pretreatment temperature, irrespective of the reductant. For the H_2 pretreated samples, increasing the pretreatment temperature increases the selectivity towards C_2–C_4 olefins and C_{5+} hydrocarbons, which we attribute to iron nanoparticle growth. Transmission electron microscopy (TEM), particle size distribution (PSD) analysis, and X-ray diffraction (XRD) illustrate that pretreatment with H_2 induces reduction of Fe_2O_3 to metallic iron, and there is observed sintering as the pretreatment temperature increases. In contrast, CO pretreatment does not result in sintering, but we observe Fe carburization and coke deposition which promotes methane (CH_4) formation. Our findings provide important insight into how pretreatment conditions affect iron particle size, phase, and zeolite properties, and in turn, FTS performance, guiding the selection of appropriate FTS pretreatment conditions for Fe-ZSM-5 catalysts.

2. Methods

Synthesis of Fe–Na-ZSM-5

The ZSM-5 zeolite was synthesized using tetrapropylammonium hydroxide (TPAOH, 25 wt%), ammonium nitrate (NH_4NO_3), aluminum nitrate nonahydrate ($Al(NO_3)_3{\cdot}9H_2O$), tetraethyl orthosilicate (TEOS), and sodium hydroxide (NaOH) which were all purchased from Alfa Aesar and used without further purification. First, 6.25 g of TEOS and 6.10 g of TPAOH were mixed in a Teflon container and stirred at 80 °C for 24 hours. After 24 hours, 0.23 g of $Al(NO_3)_3{\cdot}9H_2O$, and 0.12 g of NaOH were dissolved in 2 g of distilled water to form a solution. The solution was added dropwise into the mixture in the Teflon container. The resultant gel with a molar ratio of $1SiO_2 : 0.01Al_2O_3 : 0.25TPAOH : 0.05Na_2O : 8.3H_2O$ was then transferred to an autoclave and crystallized at 170 °C for 24 hours. The obtained solid product was washed three times using deionized water and collected by centrifugation at 13 000 rpm for 10 min. After washing, the sample was left to dry overnight in the oven at 100 °C. The dried sample was calcined at 550 °C for 10 hours to remove the TPAOH template. Then Na-form ZSM-5 (Na-ZSM-5) with Si/Al ratio 50 was obtained as the final product.

The iron supported zeolite catalyst was synthesized *via* the wetness impregnation method using iron(III) nitrate nonahydrate ($Fe(NO_3)_3{\cdot}9H_2O$), and distilled water. To obtain a 5 wt% loading of iron, 0.362 g of $Fe(NO_3)_3{\cdot}9H_2O$ was dissolved in 0.138 g of distilled water. The solution was added dropwise into 0.95 g of Na-ZSM-5 while stirring. The resulting mixture was left to dry at 30 °C, followed by calcination at 550 °C for 5 hours at 5 °C min^{-1}. The obtained catalyst was designated as Fe–Na-ZSM-5.

Temperature programmed reduction and desorption (H_2-TPR, CO-TPR, and CO-TPD)

Temperature-programmed reduction using either H_2 or CO (H_2-TPR and CO-TPR), and CO temperature-programmed desorption (CO-TPD) experiments were performed using a Micromeritics AutoChem II analyzer. For the H_2-TPR experiment, the Fe–Na-ZSM-5 catalyst was degassed in helium flow of 20 mL min^{-1} at 300 °C with a ramp rate of 10 °C min^{-1} for 1 hour. After which the sample was cooled to 35 °C, followed by introduction of H_2 at 40 mL min^{-1} and ramped to 900 °C at 10 °C min^{-1}. The same procedure was used for CO-TPR except with the replacement of H_2 by 20 mL min^{-1} CO.

For CO temperature-programmed desorption (CO-TPD) experiments, the catalysts were pretreated under 10% H_2 in Ar at 350 °C, 450 °C, 550, and 770 °C with a ramp rate of 10 °C min^{-1} for 2 h before pulsing CO over the catalyst at 35 °C. After CO adsorption, the sample was purged with helium and heated to 900 °C at a ramp rate of 5 °C min^{-1}. The same procedure was used for the CO pretreated samples with the replacement of H_2 with CO and reduction temperatures of 300 °C, 490 °C, and 750 °C.

Fischer–Tropsch synthesis reactor studies

For the reactor studies, the Fe–Na-ZSM-5 catalyst was pressed into pellets and ground between 212–315 μm. 50 mg of the catalyst was loaded into a stainless-steel reactor using quartz wool to fix the catalyst in place. The catalyst was pretreated with 40 mL min^{-1} H_2 or 20 mL min^{-1} CO at the prescribed temperatures with a ramp rate of 10 °C min^{-1} at 50 psig and held for 2 h. After pretreatment, the reactor was pressurized to 300 psig under the reductant gas and switched to the bypass loop. The bypass was pressurized to 300 psig with a combination of the reactant gases, composed of 20 mL min^{-1} H_2, 10 mL min^{-1} CO, and 15 mL min^{-1} Ar to achieve H_2/CO = 2. The reaction was run for 12 hours, and an in-line Agilent gas chromatograph equipped with a flame ionization detector (FID) and a thermal conductivity detector (TCD) was used to evaluate the concentration of gases exiting the reactor. The conversion was calculated using the Ar internal standard to account for the decreasing molar volume due to the reaction using the inlet molar flow rate of CO as the basis for the calculation. The selectivity for the carbon-containing products was calculated on a moles of carbon basis. All carbon balances close to 98 ± 0.8%.

Transmission electron microscopy (TEM)

Images of the pretreated Fe–Na-ZSM-5 catalysts were collected using a FEI Tecnai G2-F20 transmission electron microscope with a 200 kV accelerating voltage. Before imaging, the sample was either pretreated in 40 mL min^{-1} H_2 at 350 °C, 450 °C, 550 °C, or 770 °C for 2 hours with a ramp rate of 5 °C min^{-1}, or in 20 mL min^{-1} CO for 2 hours at 300 °C, 490 °C, or 750 °C with a ramp rate of 5 °C min^{-1}.

Thermogravimetric analysis (TGA)

Thermogravimetric analysis (TGA) was performed using a Discovery series TGA under a nitrogen flow rate of 25 mL min^{-1}. The sample holder was loaded into the equipment and tared, before loading the sample with a mass of 5–10 mg. The sample was heated to 110 °C with a ramp rate of 20 °C min^{-1} and held for 10 minutes to degas, before ramping to 850 °C with a ramp rate of 15 °C min^{-1}.

X-ray diffraction (XRD)

Before collecting the XRD measurements, the catalysts were affixed to a Nylon loop (0.1 mm ID) with a light coating of viscous oil. XRD data were collected on a Rigaku XtaLAB Synergy-S diffraction system equipped with a HyPix-6000HE HPC detector. CuKα radiation (λ = 1.54184 Å) was generated by a PhotonJet-S microfocus source at 50 kV, and 1 mA. At room temperature (293 K) and with a sample-to-detector distance of 34 mm, two combination ω–φ "Gandolfi" scans were performed, each for 300 s: 1) ω from −62.00 to 31.00 degrees and φ rotated through 720 degrees, at θ = −42.00 and κ = 70.00 degrees; 2) ω from −30.00 to 61.00 degrees and φ rotated through 720 degrees, at θ = 41.22 and κ = −70.00 degrees. The crystallinity of the zeolites in the as-synthesized catalysts was calculated using a method reported by Mohamed *et al.*[35] For each of the samples, the method compares the relative areas of the XRD peaks at 2θ = 22–25°. The as-synthesized Na-ZSM-5 is used as the 100% crystallinity reference.

Mössbauer analysis

^{57}Fe Mössbauer spectroscopy was used to investigate the iron phases present in the Fe–Na-ZSM-5 catalyst before and after pretreatment in H_2 *vs.* CO at each pretreatment temperature. The samples were prepared in Delrin Mössbauer sample cups under ambient conditions and frozen in liquid N_2, with an inner Delrin cup added before freezing. Low-temperature measurements at 80 K were performed using a SeeCo. MS4 Mössbauer spectrometer integrated with a Janis SVT-400 T He/N_2 cryostat, and isomer shifts were referenced to α-Fe at 25 °C. Spectral data were analyzed using WMoss (SeeCo), with raw data (black dots) and fits (black line), including individual components represented by colored hyperfine patterns. The fitting errors were δ ± 0.02 mm s^{-1} and ΔE_Q ± 3%, while quantification errors for multicomponent fits were ± 3%. Abbreviations used include full width at half maximum (FWHM), isomer shift (δ), electric quadrupole splitting (ΔE_Q), and internal magnetic field (H_{int} (kG)).

BET surface area measurements

N_2 physisorption experiments were performed using a Micromeritics ASAP 2020 sorption analyzer at −196 °C. Prior to the analysis, all samples were degassed at 350 °C for 2 hours under vacuum, and 97 points were analyzed. The surface area of the samples was determined using the Brunauer–Emmett–Teller (BET) method.

X-ray absorption fine structure (XAFS)

In situ XAFS measurements were conducted to investigate the structural changes of iron during temperature programmed reduction (TPR), pretreatment, and FTS. The measurements were performed at the 8-ID (ISS) beamline at the National Synchrotron Light Source (NSLS-II), Brookhaven National Laboratory. The description of the beamline can be found in the literature.[36] The monochromator energy was calibrated by setting the position of the Fe foil X-ray absorption spectroscopy (XAS) spectrum derivative maximum to 7112 eV. The fluorescence signal from the sample was collected using

a photodiode equipped with a Mn filter. The as-synthesized Fe–Na-ZSM-5 was diluted with boron nitride in a 1:5 ratio. The mixture was ground together and pressed to form pellets. Then the pellets were grounded and sieved at a 212–315 μm mesh size before loading into a quartz glass capillary tube with 1.5 mm outer diameter and 10 μm wall thickness. The loaded tube was mounted within a custom-designed Claussen cell. *In situ* CO-TPR and H_2-TPR were performed while XAFS data of Fe K-edge were collected. CO and H_2 flowrate were 3 and 6 mL min^{-1} respectively, maintaining the 1:2 CO:H_2 ratio (20 mL min^{-1} CO and 40 mL min^{-1}) used for H_2-TPR, CO-TPR, and during pretreatment prior to FTS reaction in the main reactor.

Ex situ XAFS data were collected for iron oxide standards (Fe_2O_3, Fe_3O_4, FeO, and Fe). Before the measurements, the iron standards were diluted in boron nitride to obtain 5 wt% of the standards, similar to the weight percent of iron present in Fe–Na-ZSM-5. Iron carbide references were synthesized *in situ* using a method reported by De Smit *et al.*[37] Diluted Fe_2O_3 was loaded into the capillary tube and mounted on the custom-designed Claussen cell. 3 mL min^{-1} of CO was introduced into the system, and the temperature was ramped to 350 °C for Fe_5C_2 and 450 °C for Fe_3C synthesis at a ramp rate of 2 °C min^{-1} and held for 2 hours. *In situ* XAFS data were collected during the carbide synthesis. For all the measurements, the incident and transmitted X-ray signals were recorded using ionization chambers, while fluorescence signals were captured with a passivated implanted planar silicon (PIPS) detector. Calibration against the standards and data analysis were performed using the Demeter 0.9.26 package (Athena).

The MCR analysis of the *in situ* XANES data was carried out using the pyMCR package described in the literature and is consistent with our previous work.[38,39] Briefly, the number of components necessary to reproduce the XANES spectral series for each dataset was determined based on the autocorrelation analysis of the singular vectors obtained using the singular value decomposition of the corresponding data matrices. Then, the alternating least squares MCR fitting was applied to the data using the appropriate reference spectra as starting solutions. The fitting was carried out with non-negativity constraints on both spectral and concentration profiles, a normalization constraint on the concentrations such that the sum of all component concentrations adds up to unity at each time point, as well as an additional cut-off constraint that removes component contributions if it is below 0.02, which was found to improve the stability of the fitting. The converged results were then used for the analysis.

3. Results and discussion

3.1 FTS performance of the pretreated Fe–Na-ZSM-5 catalysts

FTS performance as a function of pretreatment conditions over Fe–Na-ZSM-5 is shown in Fig. 1 with tabulated values included in Table S1.† The samples are denoted as H_2-*T* for the H_2-pretreated samples, and CO-*T* for the CO-pretreated samples, where *T* represents the pretreatment temperature. In accordance with the H_2 temperature programmed reduction (H_2-TPR) in Fig. S1(a)† which shows three peaks centered at *ca.* 350, 550, and 770 °C, we pretreated Fe–Na-ZSM-5 in H_2 at each of the three temperatures and labeled the catalysts H_2-350, H_2-550, and H_2-770. 450 °C pretreatment temperature (H_2-450) is also included because it is a commonly used pretreatment temperature for iron-based catalysts during FTS.[40,41] For the H_2-pretreated catalysts in Fig. 1(a), increasing the pretreatment temperature from 350 °C to 770 °C decreases the CO conversion from 10.8 to 3.4%. We hypothesize that sintering of iron particles reduces available active iron surface area and phase transitions to less-active Fe result in the decrease in measured activity. For the product distribution, increasing the pretreatment temperature under H_2 increases C_2–C_4 olefins and C_{5+} hydrocarbons, whereas C_2–C_4 paraffins and CH_4 decrease. These findings are consistent with sintering, where previous literature reports indicating that large Fe nanoparticles promote formation of C_{5+} hydrocarbons,[24,42,43] and smaller iron particles are associated with increased CH_4 selectivity.[43] As shown in Table S1,† increasing pretreatment temperature

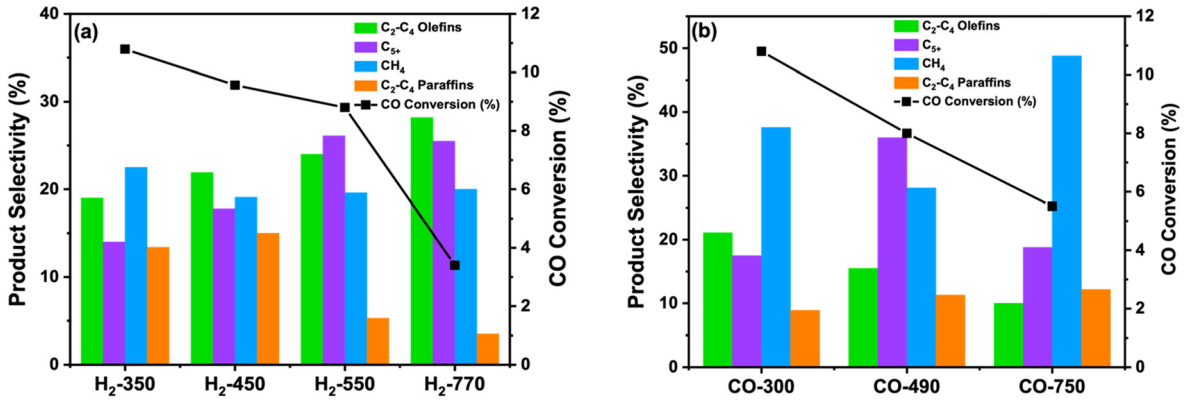

Fig. 1 CO conversion and hydrocarbon selectivity averaged between 9–12 hours on stream of Fe–Na-ZSM-5 pretreated in H_2 (a) and CO (b) at temperatures ranging from 300–770 °C. Reaction conditions: catalyst mass = 50 mg, temperature = 300 °C, pressure = 300 psig, H_2/CO = 2, H_2 = 20 mL min^{-1}, CO = 10 mL min^{-1}, and Ar = 15 mL min^{-1} as internal standard.

generally decreases CO_2 selectivity from 31.1% in H_2-350 to 22.9% in H_2-770.

Fig. 1(b) shows the FTS performance of the CO-pretreated samples, with three pretreatment temperatures selected (300, 490, and 750 °C), in accordance with CO temperature-programmed reduction (CO-TPR) in Fig. S1(b).† Similar to the H_2-pretreated samples, increasing the pretreatment temperature also results in decreasing CO conversion from 10.8 to 5.5%, likely because of sintering, iron phase transformations, and/or carbon deposition. Although increasing CO pretreatment temperatures enhances carburization, which can be favorable for FTS, the higher temperatures may lead to carbon deposition, which blocks active sites and decreases activity.[13,44] The product selectivity in Fig. 1(b) shows a trend with C_2–C_4 olefins and paraffins, where olefins decrease and paraffins slightly increase with increasing pretreatment temperatures. At the highest pretreatment temperature, CH_4 selectivity dominates possibly due to the removal of deposited carbon as CH_4. The CO-pretreated samples have lower CO_2 selectivity when compared to the H_2-pretreated samples, showing values of 14.8, 9.3, and 10.1% for CO-300, CO-490, and CO-750, respectively. Understanding the observed trends in FTS performance requires deeper investigation into the structure of the catalysts after pretreatment.

3.2 Structural properties of the pretreated Fe–Na-ZSM-5 catalysts

The effect of pretreatment temperature on the iron particle size is first investigated using transmission electron microscopy (TEM) and thermogravimetric analysis (TGA) in Fig. 2. The particle size distribution (PSD) of the H_2-pretreated samples in Fig. 2(a–d) shows a shift towards higher values with increasing pretreatment temperatures, indicating Fe sintering is occurring. These findings are in agreement with literature and could be contributing to the decreased FTS activity in Fig. 1(a).[7,15,17,18,45–47] In contrast, there is no significant increase in iron particle size for the CO-pretreated samples in Fig. 2(e–g), possibly due to carburization and carbon deposition stabilizing the Fe nanoparticles, consistent with observations by other researchers.[7,10,45] For the highest temperature pretreated sample, CO-750, carbonaceous layers are observed around

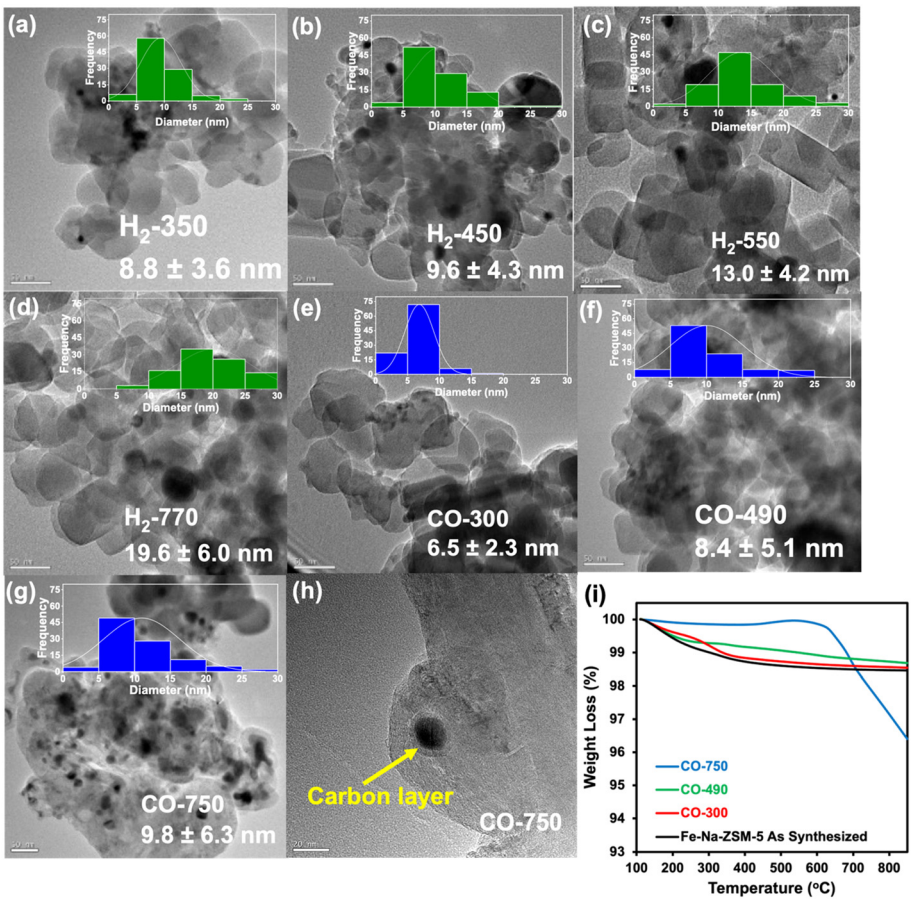

Fig. 2 Transmission electron microscopy (TEM) images, and particle size distribution (PSD) of Fe–Na-ZSM-5 pretreated in H_2 at 350 °C (a), 450 °C (b), 550 °C (c), 770 °C (d), and in CO at 300 °C (e), 490 °C (f), and 750 °C (g and h). Thermogravimetric analysis (TGA) of the CO-pretreated samples (i). TGA of the H_2-pretreated samples is in Fig. S2 of the ESI.† The PSD was generated using diameter measurements of 100 iron particles from the TEM images.

Table 2 Physical properties of Fe–Na-ZSM-5 pretreated in H_2 and CO as a function of pretreatment temperature with as-synthesized Na-ZSM-5 and Fe–Na-ZSM-5 included as references

Catalyst	Iron median size (nm)	BET surface area ($m^2\ g^{-1}$)	Total pore volume ($cm^3\ g^{-1}$)	Micropore volume ($cm^3\ g^{-1}$)	Relative zeolite crystallinity (%)
Na-ZSM-5[a]	NA	352	0.66	0.12	100.0
Fe–Na-ZSM-5[a]	NA	331	0.61	0.11	88.5
H_2-350	8.8 ± 3.6	295	0.55	0.10	90.0
H_2-450	9.6 ± 4.3	340	0.63	0.11	87.5
H_2-550	13.0 ± 5.2	335	0.59	0.10	83.7
H_2-770	19.6 ± 6.0	161	0.39	0.05	81.2
CO-300	6.5 ± 2.3	294	0.57	0.10	91.8
CO-490	8.4 ± 5.1	260	0.50	0.08	83.1
CO-750	9.8 ± 6.3	205	0.58	0.06	82.8

[a] As-synthesized samples.

the iron particles in the TEM image (Fig. 2(h)), which is further supported by the TGA in Fig. 2(i) showing a sharp decrease in mass, suggestive of coke removal. This trend is not observed in the H_2-pretreated catalysts in Fig. S2,† indicating that carbon deposition is not contributing to the decrease in activity of the H_2-pretreated catalysts with increasing temperature. However, because the CO-pretreated samples do not exhibit significant sintering, the decrease in CO conversion with increasing pretreatment temperature is attributed to changes in the Fe phase and carbon deposition.

Following the observed iron sintering and coke deposition on the pretreated catalysts, the effect of the pretreatment temperature on the surface area, porosity, and pore volume of ZSM-5 is measured with N_2 physisorption and included in Table 2. After iron impregnation, the initial surface area and total pore volume of the parent Na-ZSM-5, initially measured as 352 $m^2\ g^{-1}$ and 0.66 $cm^3\ g^{-1}$, respectively, decreases to 331 $m^2\ g^{-1}$ and 0.61 $cm^3\ g^{-1}$. This decrease is attributed to the obstruction of zeolite pores by the iron nanoparticles, leading to decreased accessible zeolite surface area.[48] For the H_2-pretreated samples at the lowest pretreatment temperature (H_2-350), the surface area and total pore volume decrease to 295 $m^2\ g^{-1}$ and 0.55 $cm^3\ g^{-1}$, respectively. For H_2-450 and H_2-550, the surface area and pore volume exhibit slight changes. At the highest pretreatment temperature (H_2-750), the surface area decreases to 161 $m^2\ g^{-1}$, and the total pore and

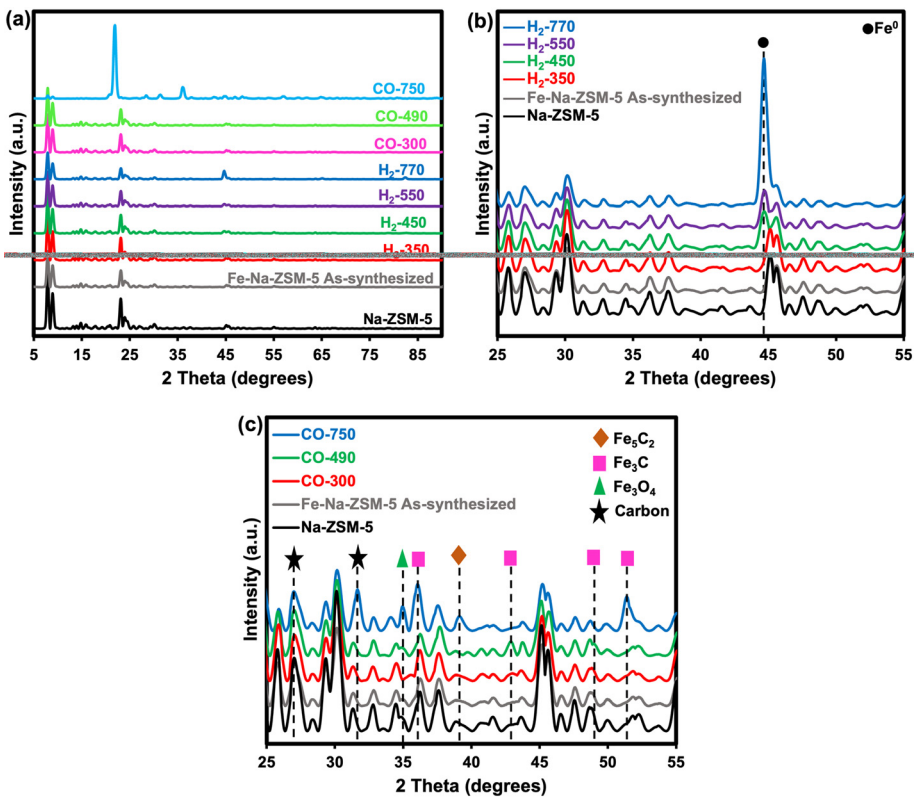

Fig. 3 X-ray diffraction (XRD) patterns of Fe–Na-ZSM-5 pretreated in H_2 and CO (a), zoomed-in XRD pattern of the H_2-pretreated samples (b), and zoomed-in patterns of the CO-pretreated samples (c).

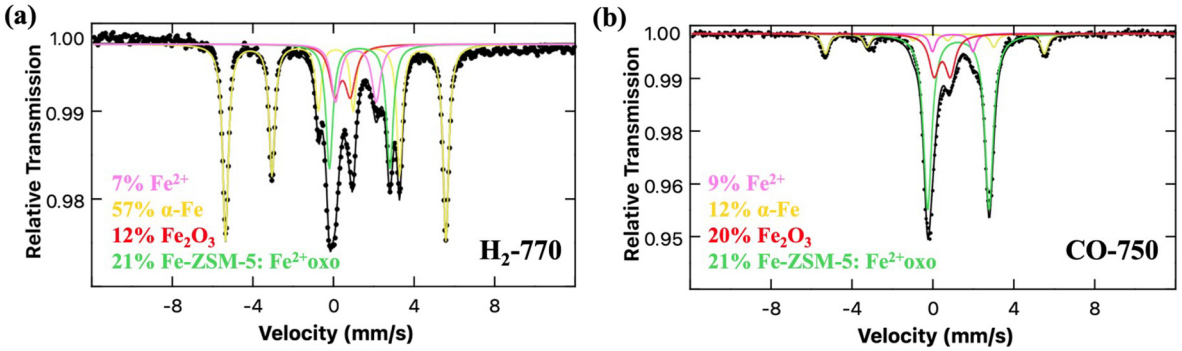

Fig. 4 Mössbauer spectra of Fe–Na-ZSM-5 pretreated in (a) H_2 at 770 °C and (b) CO at 750 °C.

micropore volumes decrease. The substantial reduction in the surface area of H_2-770 is attributed to sintering of iron particles obstructing zeolite pores, thereby blocking accessible N_2 adsorption area, or decomposition of the zeolite structure under high-temperature conditions. For the CO-pretreated samples, as the pretreatment temperature increases the BET surface area decreases from 294 to 205 $m^2\ g^{-1}$ likely due to the blocking of zeolite pores by deposited carbon.

X-ray diffraction (XRD) patterns of the pretreated samples in Fig. 3 provide insight into the crystallinity of the ZSM-5 and the iron structure post-pretreatment. The XRD patterns of all the pretreated samples in Fig. 3(a) show preservation of the bulk crystalline structure of ZSM-5 with characteristic peaks of the MFI zeolite after pretreatment, which is consistent with TEM and studies showing that the bulk crystalline structure of the zeolite remains stable up to 800 °C.[49] The relative crystallinity of ZSM-5 is calculated from the XRD patterns using a method reported by Mohamed *et al.*[35] with as-synthesized Na-ZSM-5 used as the 100% crystallinity reference. As shown in Table 2, increasing the pretreatment temperature leads to a slight decrease in the relative crystallinity of the ZSM-5 zeolite irrespective of the reductant (CO or H_2). This suggests that the bulk crystalline structure of the ZSM-5 is mostly preserved after high-temperature pretreatment (≤770 °C) with a slight decrease in relative crystallinity.

To analyze observable iron species, we provide zoomed-in XRD profiles of the catalysts within the 2θ range of 25–55° in Fig. 3(b and c). Overall, the XRD shows that pretreatment in H_2 leads to the complete reduction of Fe_2O_3 to Fe^0, also supported by the H_2-TPR in Fig. S1(a),† while CO pretreatment results in the simultaneous reduction and carburization of Fe_2O_3, which forms iron carbides and reduced oxides. In the case of H_2-770, we observe a significant increase at 44.7°, corresponding to the (110) plane of metallic iron (Fe^0), suggesting Fe agglomeration begins at 450 °C which is consistent with the TEM images.[50,51] This aggregation may be responsible for the very low CO conversion of H_2-770 as seen in Fig. 1(a). However, for the CO-pretreated samples in Fig. 3(c), agglomeration of Fe^0 peaks is absent, supporting the hypothesis that iron particles are stabilized during carburization, as suggested by TEM and PSD. Characteristic peaks are observed of Fe_3O_4(310) at 35°,[52] iron carbides (Fe_5C_2, Fe_3C) at 36.1, 39.2, and 51.5°,[53,54] and carbon at 27.0 and 31.6°. Iron carbides, such as Fe_5C_2 and Fe_3C are active phases for CO conversion, with Fe_5C_2 frequently cited as the phase that promotes hydrocarbon formation.[37,40,41,55,56]

The iron phase composition of the pretreated Fe–Na-ZSM-5 samples was analyzed further using Mössbauer spectroscopy, as shown in Fig. 4 and S3.† The Mössbauer spectra of the high-temperature pretreatment samples, H_2-

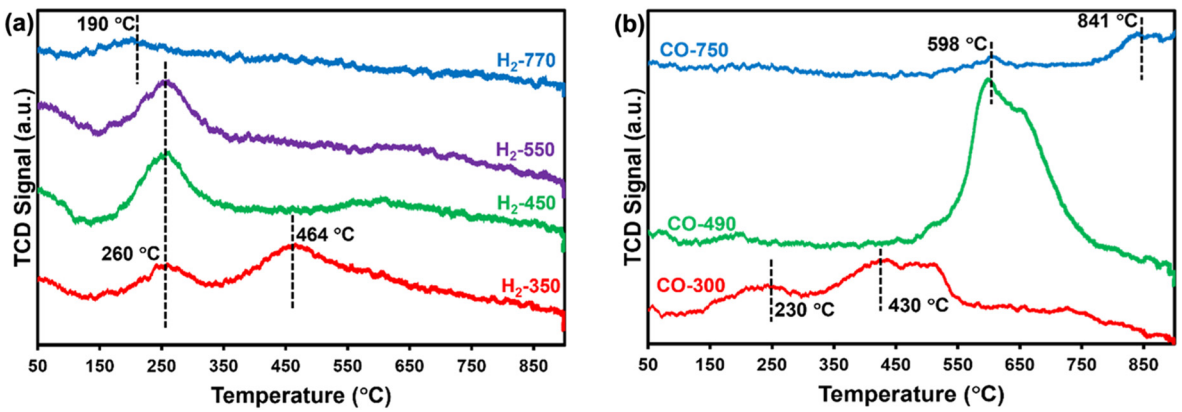

Fig. 5 Carbon monoxide temperature programmed desorption (CO-TPD) of the Fe–Na-ZSM-5 catalysts pretreated in H_2 (a) and CO (b) at different temperatures.

770 and CO-750 are shown in Fig. 4. The spectra of H_2-770 indicate that the sample primarily contains metallic iron in the form of α-Fe (57%), which agrees with the sintered metallic iron observed by XRD. Additionally, 21% of the iron is present as Fe^{2+} oxo suggesting integration into the zeolite framework due to the high-temperature pretreatment. The Mössbauer of the CO-750 sample shows that the majority of the iron (65%) is also present as Fe^{2+} oxo, likely due to the high pretreatment temperature, while only about 12% is present as metallic iron. The Mossbauer spectra of CO-300 and CO-490 in Fig. S3† show a complex mixture of iron phases that are predominantly Fe^{2+} including oxides and carbides. The Mossbauer fitting parameters are summarized in Tables S4 and S5.†[40,57,58]

3.3 CO adsorption properties of the pretreated Fe–Na-ZSM-5 catalysts

To gain a better understanding of the effect of pretreatment conditions on the Fe structure, we include CO temperature programmed desorption (CO-TPD) in Fig. 5. The CO-TPD of the H_2-pretreated samples in Fig. 5(a) highlights the effect of iron particle size on CO adsorption. In the CO-TPD of the H_2-pretreated samples, peaks at 190 °C and 260 °C are attributed to desorption of weakly bound CO, while the peak at 464 °C is attributed to strong CO binding, indicative of CO dissociation.[59–61] At higher pretreatment temperatures (450–770 °C), CO preferentially binds weakly, whereas, for H_2-350, CO exhibits both weak and strong binding, suggesting the presence of two active sites in H_2-350. The CO-TPD profiles of the H_2-pretreated samples suggest that as pretreatment temperature increases, the CO adsorption and dissociative capacity decrease. This is attributed to the smaller particle size at low pretreatment temperatures, providing more active sites and higher electron density for CO adsorption,[62] as supported by the FTS data presented in Fig. 1(a).

The CO-TPD of the CO-pretreated samples shown in Fig. 5(b) highlights the effect of iron carbide formation and coke deposition on CO adsorption. For the CO-pretreated samples, peaks for weak and strong binding of CO are present in the CO-TPD of CO-300, which is similar to H_2-350. The similarity in the CO adsorption behavior of CO-300 and H_2-350 suggests the presence of similar active sites which could be responsible for the similarity in CO conversion as shown in Fig. 1. Interestingly, the BET surface area and pore volume of these two samples are also similar as shown in Table 2.

For the CO-TPD of CO-490 and CO-750, a peak at 598 °C is attributed to the desorption of CO bound to iron carbides.[63] The absence of the peak at 598 °C for CO-300 indicates that there is less CO dissociation, and in turn, iron carbide formation at pretreatment temperatures below 490 °C. The lack of peaks over CO-750 is attributed to carbon deposition on the active sites, supported by the TGA in Fig. 2(i). In summary, the CO-TPD shows that CO adsorption is weakened by larger iron particle sizes because the desorption profiles of the catalysts with smaller particle sizes, *i.e.* the CO-pretreated samples and H_2-350 exhibit desorption at high temperatures, consistent with findings by Suo *et al.*[64]

3.4 Structure–performance relationships of the pretreated catalysts

To investigate the effect of pretreatment on FTS performance, CO conversion *versus* time on stream (TOS) data for all the pretreated catalysts is included in Fig. 6. The 12-hour TOS results for H_2-350 and H_2-450 in Fig. 6(a) exhibit similar trends with high initial activity. After about 4 h on stream, the activity of H_2-350 increases while that of H_2-450 remains relatively stable. The initial decline in activity of both catalysts may be attributed to the transformation of iron oxides and/or metallic iron into iron carbides and deposition of inactive graphitic carbon.[25,28,65] Luo *et al.*[25] report that in H_2-pretreated iron catalysts, after the induction period, the formation of iron carbides increases slightly with reaction

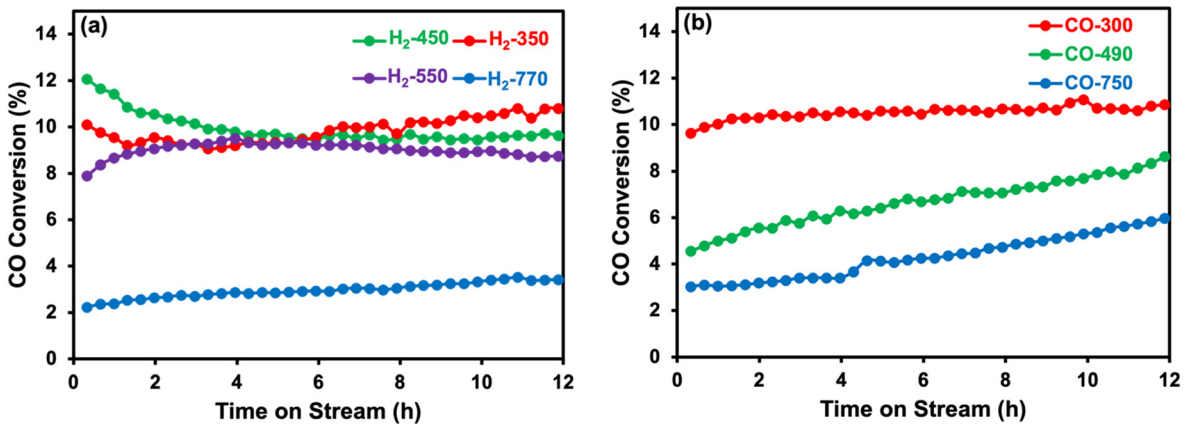

Fig. 6 CO conversion *versus* time on stream of Fe–Na-ZSM-5 as a function of pretreatment temperature in H_2 (a), and in CO (b). Reaction conditions: catalyst mass = 50 mg, temperature = 300 °C, pressure = 300 psig, H_2/CO ratio = 2, H_2 = 20 mL min^{-1}, CO = 10 mL min^{-1}, and Ar = 15 mL min^{-1} as internal standard.

time, resulting in the gradually increasing CO conversion, agreeing with our observations and previous studies on Fe–Na-ZSM-5.[40,41] For the higher pretreatment temperatures (H_2-550 and H_2-770), the catalysts interestingly do not exhibit the initial decrease in activity, possibly due to sintering and an induction mechanism that is a function of the larger Fe particle size.

The 12-hour TOS results for the CO-pretreated samples in Fig. 6(b), show distinct behavior compared to H_2-pretreated samples because there is not a decrease in initial activity. These findings are consistent with those of Xu *et al.*[66] where they observe an initial decline in the CO conversion of the H_2 pretreated catalyst, which is absent in the CO and CO/H_2 pretreated catalysts. Our reactor data suggests that CO pretreatment of Fe–Na-ZSM-5 at 490 °C and 750 °C induces a higher degree of carburization and coke deposition on the iron oxide particles, resulting in lower conversion. However, as the reaction proceeds the coke is removed that reveals active sites, which gradually increases the CO conversion.

To elucidate details of the iron structure during pretreatment as a function of pretreatment conditions, X-ray absorption fine structure (XAFS) analysis is conducted on H_2-350, H_2-450, CO-300, and CO-490. The K-edge X-ray absorption near-edge structure (XANES) analysis after pretreatment is shown in Fig. 7 with the insets showing the pre-edge features, and the as-synthesized Fe–Na-ZSM-5 is included as a reference. Spectra for iron standards Fe_2O_3, Fe_3O_4, FeO, and Fe^0 are included in Fig. S4.† The XANES spectrum of the as-synthesized Fe–Na-ZSM-5 shows a pre-edge feature at 7115 eV and white line at 7134.4 eV consistent with the Fe_2O_3 reference in Fig. S4,† indicating that Fe_2O_3 is present in the Fe–Na-ZSM-5 catalyst before pretreatment. The XANES spectra of all the samples in Fig. 7 shift to lower energies after pretreatment in either H_2 or CO at all temperatures. For instance, the white line of H_2-350 appears at 7130.2 eV with pre-edge at 7113.6 eV, which are at lower energies than those of the as-synthesized Fe–Na-ZSM-5 catalyst. For all the samples, the intensities of the higher pretreatment temperatures (H_2-450 and CO-490) are lower compared to the lower pretreatment temperatures, suggesting a higher degree of reduction/carburization (Fig. 7).

To gain additional insight from the *in situ* XANES data, we applied multivariate curve resolution (MCR) analysis as shown in Fig. 8(a–d). The MCR analysis was used to extract the fractions of different Fe species contained in the sample as a function of time during the pretreatment. During the analysis, we attempted to use Fe_2O_3 and Fe_3O_4 spectra as starting solutions, however, the resulting components either converged to the Fe–Na-ZSM-5 spectrum, taken prior to pretreatment, or to a non-physical spectrum. Consequently, these species are excluded from the MCR plots and only the as-is Fe–Na-ZSM-5, metallic Fe, and FeO spectra are used during the analysis. For the low-temperature pretreated samples, H_2-350 and CO-300 as depicted in Fig. 8(a and c), the Fe–Na-ZSM-5 initially undergoes gradual reduction, leading to the formation of FeO, as evidenced by the concurrent gradual

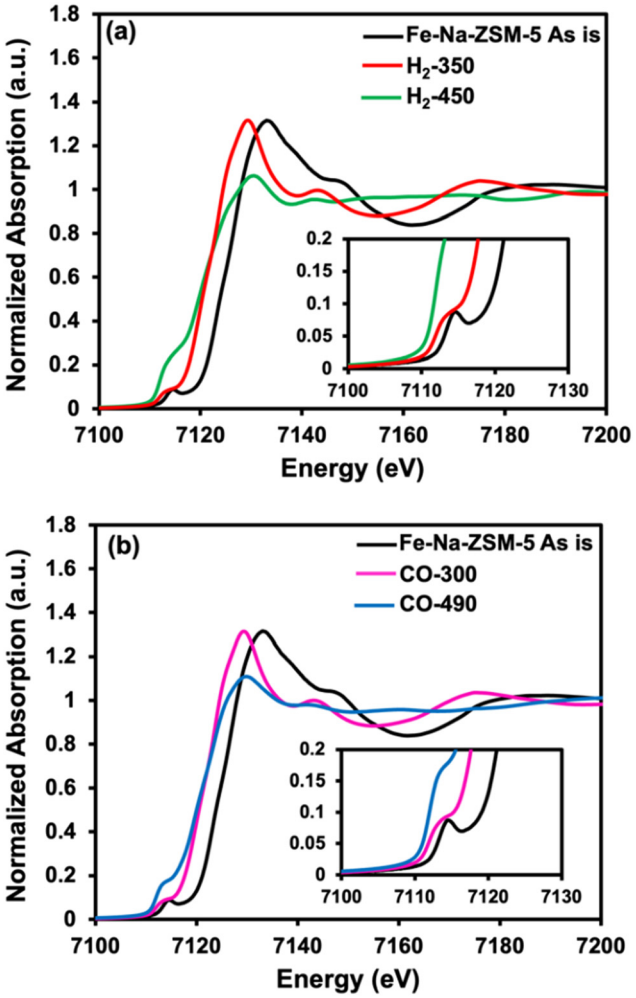

Fig. 7 Fe K-edge X-ray absorption near-edge structure (XANES) spectra with the insets showing the pre-edge features of H_2-pretreated (a), and CO-pretreated (b) Fe–Na-ZSM-5 samples. The as-synthesized catalyst, Fe–Na-ZSM-5 is included as a reference.

increase in the FeO spectrum. After about 0.8 h, the proportion of FeO within the samples stabilizes and persists until the end of the pretreatment period, indicating that FeO predominates as the primary species after pretreatment. The MCR analysis indicates that FeO is the predominant iron species in H_2-350 and CO-300 after pretreatment.

The comparable fractions of FeO shown by the MCR analysis of H_2-350 and CO-300, alongside the analogous CO-TPD profiles as depicted in Fig. 5, likely account for the similar CO conversion observed in Fig. 1. However, the presence of iron carbides in CO-300 suggested by the additional shoulder in its CO-TPD at ~500 °C, likely contribute to the differences in the initial catalyst activity, as evidenced in the TOS data in Fig. 6(a and b), as well as differences in product selectivity. We hypothesize that at the onset of the reaction, the predominant FeO in H_2-350 undergoes transformation, forming a mixed phase of iron containing some iron carbides and inactive carbides. After ~2 hours on stream, the CO conversion gradually increases,

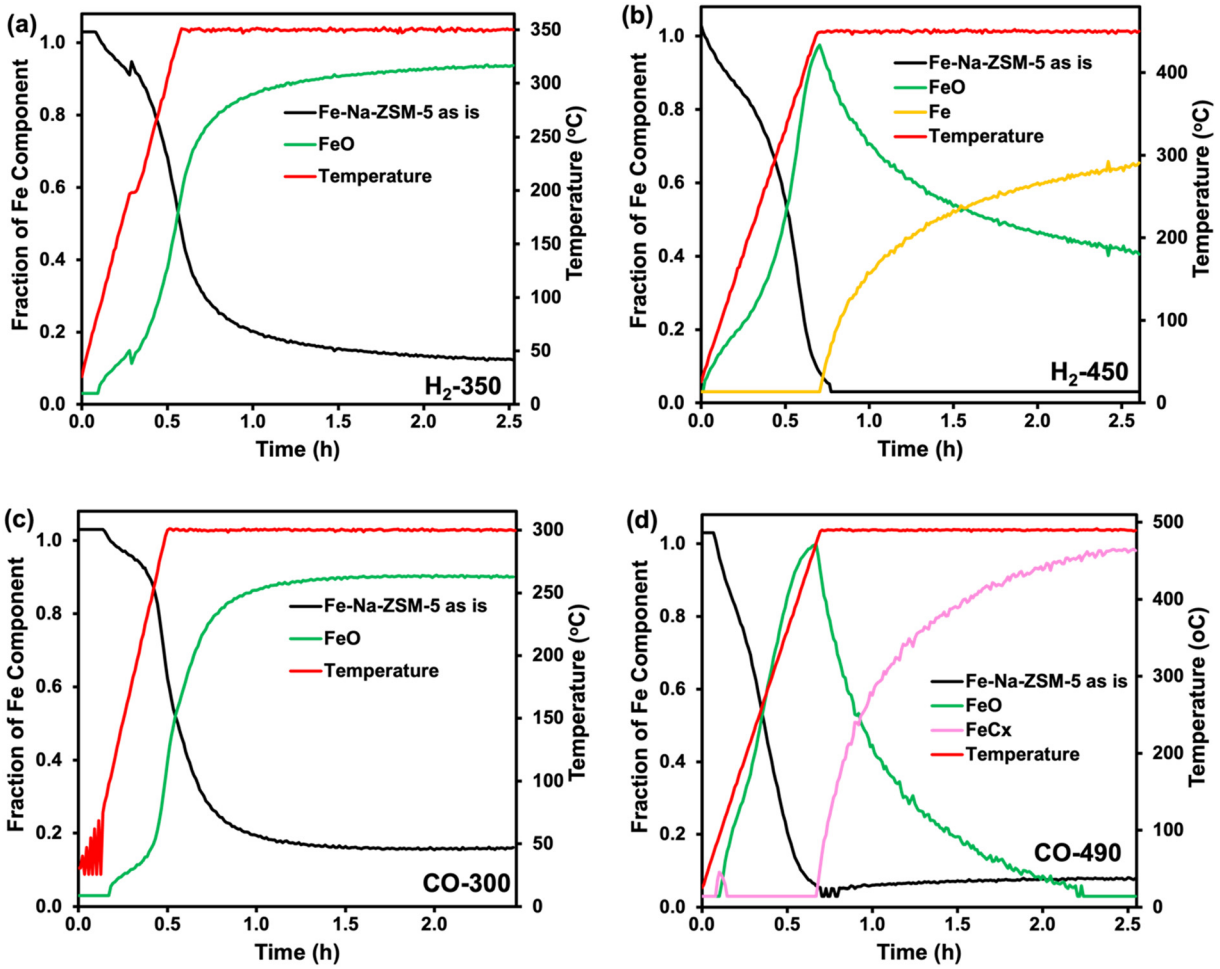

Fig. 8 Multivariate curve resolution (MCR) analysis of the XANES spectra of Fe–Na-ZSM-5 pretreated in H_2 at 350 °C (a), and 450 °C (b) and in CO at 300 °C (c), and 490 °C (d), with the as-synthesized catalyst, Fe–Na-ZSM-5 included as a reference.

mirroring the TOS pattern of CO-300, which likely already contains iron carbides prior to FTS.

In the MCR analysis of H_2-450 shown in Fig. 8(b), the fraction of FeO steadily increases as that of iron oxides in as-synthesized Fe–Na-ZSM-5 gradually decreases. After about 0.7 h, some of the generated FeO undergoes further reduction, forming metallic Fe. The fractional contribution of Fe gradually increases, ultimately becoming the predominant species post-pretreatment. The appearance of Fe seems to coincide with pretreatment temperatures above 400 °C, which agrees with the XRD data in Fig. 3(b). Similarly, for CO-490 in Fig. 8(d), the fraction of iron oxides in the as-synthesized Fe–Na-ZSM-5 gradually decreases during reduction, facilitating the formation of FeO with increasing fractional contribution. However, after ~0.7 h, a spectrum indicative of a mixed phase emerges. Here, successful fitting of the data was accomplished by adding an additional spectrum from the end of the *in situ* XANES series to the MCR starting solutions. We hypothesize that the extracted component represents a mixed phase and can be attributed to iron carbides, and some iron oxides which gradually increase in concentration during pretreatment. Overall, the MCR analysis agrees with XRD, suggesting that higher pretreatment temperatures promote the reduction and carburization of Fe in Fe–Na-ZSM-5.

Conclusion

This study explores the effect of pretreatment conditions on the structure and performance of iron supported on ZSM-5 (Fe–Na-ZSM-5) for FTS. The reactor studies and structural characterization show that pretreatment in H_2 leads to sintering, diminishing CO adsorption capacity and CO conversion at high temperatures, while CO pretreatment induces carbide formation and coke deposition, stabilizing iron particles but lowering CO conversion at higher reduction temperatures. Irrespective of activation gas, the pretreatment temperature significantly affects the initial iron phase and further *in situ* restructuring that occurs as the reaction progresses, yielding comparable trends in the TOS data across all catalysts pretreated with the same gas. However, the variation in the fractions of the iron phases present according to the XAFS data may account for differences in the FTS performance.

Data availability

The data supporting this article have been included as part of the ESI.†

Conflicts of interest

There are no conflicts of interest to declare.

Acknowledgements

We gratefully acknowledge funding by the National Science Foundation (CBET-2345734). This research used resources of the 8-ID Inner Shell Spectroscopy beamline of the National Synchrotron Light Source II, a U.S. Department of Energy (DOE) Office of Science User Facility operated for the DOE Office of Science by Brookhaven National Laboratory under Contract No. DE-SC0012704.

References

1 K. Keyvanloo, M. K. Mardkhe, T. M. Alam, C. H. Bartholomew, B. F. Woodfield and W. C. Hecker, Supported iron Fischer–Tropsch catalyst: superior activity and stability using a thermally stable silica-doped alumina support, *ACS Catal.*, 2014, **4**(4), 1071–1077.

2 Y. Xue, Z. Liu, Y. Zhang, S. Duan and J. Chen, Effect of the Valence State of Iron in the Precursors on the Fischer–Tropsch Synthesis Performance of an Fe/Fe Foam Catalyst, *Ind. Eng. Chem. Res.*, 2021, **60**(6), 2410–2417.

3 S. Abelló and D. Montané, Exploring iron-based multifunctional catalysts for Fischer–Tropsch synthesis: a review, *ChemSusChem*, 2011, **4**(11), 1538–1556.

4 C.-F. Huo, Y.-W. Li, J. Wang and H. Jiao, Insight into CH4 formation in iron-catalyzed Fischer–Tropsch synthesis, *J. Am. Chem. Soc.*, 2009, **131**(41), 14713–14721.

5 B. H. Davis, Fischer–Tropsch synthesis: reaction mechanisms for iron catalysts, *Catal. Today*, 2009, **141**(1–2), 25–33.

6 R. A. Dictor and A. T. Bell, Fischer-Tropsch synthesis over reduced and unreduced iron oxide catalysts, *J. Catal.*, 1986, **97**(1), 121–136.

7 G. Bian, A. Oonuki, N. Koizumi, H. Nomoto and M. Yamada, Studies with a precipitated iron Fischer-Tropsch catalyst reduced by H2 or CO, *J. Mol. Catal. A: Chem.*, 2002, **186**(1–2), 203–213.

8 M. Ding, Y. Yang, B. Wu, T. Wang, H. Xiang and Y. Li, Effect of reducing agents on microstructure and catalytic performance of precipitated iron-manganese catalyst for Fischer–Tropsch synthesis, *Fuel Process. Technol.*, 2011, **92**(12), 2353–2359.

9 L. Cano, M. Cagnoli, N. Fellenz, J. Bengoa, N. Gallegos, A. Alvarez and S. Marchetti, Fischer-Tropsch synthesis. Influence of the crystal size of iron active species on the activity and selectivity, *Appl. Catal., A*, 2010, **379**(1–2), 105–110.

10 K. Cheng, M. Virginie, V. V. Ordomsky, C. Cordier, P. A. Chernavskii, M. I. Ivantsov, S. Paul, Y. Wang and A. Y. Khodakov, Pore size effects in high-temperature Fischer-Tropsch synthesis over supported iron catalysts, *J. Catal.*, 2015, **328**, 139–150.

11 Y. Jin and A. K. Datye, Phase transformations in iron Fischer–Tropsch catalysts during temperature-programmed reduction, *J. Catal.*, 2000, **196**(1), 8–17.

12 H.-Y. Lin, Y.-W. Chen and C. Li, The mechanism of reduction of iron oxide by hydrogen, *Thermochim. Acta*, 2003, **400**(1–2), 61–67.

13 W. Jozwiak, E. Kaczmarek, T. Maniecki, W. Ignaczak and W. Maniukiewicz, Reduction behavior of iron oxides in hydrogen and carbon monoxide atmospheres, *Appl. Catal., A*, 2007, **326**(1), 17–27.

14 M. N. A. Tahari, F. Salleh, T. S. T. Saharuddin, A. Samsuri, S. Samidin and M. A. Yarmo, Influence of hydrogen and carbon monoxide on reduction behavior of iron oxide at high temperature: Effect on reduction gas concentrations, *Int. J. Hydrogen Energy*, 2021, **46**(48), 24791–24805.

15 R. J. O'Brien, L. Xu, R. L. Spicer and B. H. Davis, Activation Study of Precipitated Iron Fischer–Tropsch Catalysts, *Energy Fuels*, 1996, **10**(4), 921–926.

16 D. B. Bukur, M. Koranne, X. Lang, K. Rao and G. P. Huffman, Pretreatment effect studies with a precipitated iron Fischer-Tropsch catalyst, *Appl. Catal., A*, 1995, **126**(1), 85–113.

17 D. B. Bukur, X. Lang and Y. Ding, Pretreatment effect studies with a precipitated iron Fischer–Tropsch catalyst in a slurry reactor, *Appl. Catal., A*, 1999, **186**(1–2), 255–275.

18 D. B. Bukur, X. Lang, J. A. Rossin, W. H. Zimmerman, M. P. Rosynek, E. B. Yeh and C. Li, Activation studies with a promoted precipitated iron Fischer-Tropsch catalyst, *Ind. Eng. Chem. Res.*, 1989, **28**(8), 1130–1140.

19 S. Soled, E. Iglesia and R. Fiato, Activity and selectivity control in iron catalyzed Fischer-Tropsch synthesis: The influence of iron catalyst phase on slurry Fischer-Tropsch reaction pathways; Selective synthesis of alpha-olefins, *Catal. Lett.*, 1990, **7**, 271–280.

20 M. N. A. Tahari, F. Salleh, T. S. T. Saharuddin, N. Dzakaria, A. Samsuri, M. W. M. Hisham and M. A. Yarmo, Influence of hydrogen and various carbon monoxide concentrations on reduction behavior of iron oxide at low temperature, *Int. J. Hydrogen Energy*, 2019, **44**(37), 20751–20759.

21 J.-l. Zhang, L.-h. Ma, S.-b. Fan, T.-S. Zhao and Y.-h. Sun, Synthesis of light olefins from CO hydrogenation over Fe–Mn catalysts: Effect of carburization pretreatment, *Fuel*, 2013, **109**, 116–123.

22 X. Cui, J. Xu, C. Zhang, Y. Yang, P. Gao, B. Wu and Y. Li, Effect of pretreatment on precipitated Fe–Mo Fischer–Tropsch catalysts: Morphology, carburization, and catalytic performance, *J. Catal.*, 2011, **282**(1), 35–46.

23 H. W. Pennline, M. F. Zarochak, J. M. Stencel and J. R. Diehl, Activation and promotion studies in a mixed slurry reactor with an iron-manganese Fischer-Tropsch catalyst, *Ind. Eng. Chem. Res.*, 1987, **26**(3), 595–601.

24 A. Alayat, D. Mcllroy and A. G. McDonald, Effect of synthesis and activation methods on the catalytic properties of silica nanospring (NS)-supported iron catalyst for Fischer-Tropsch synthesis, *Fuel Process. Technol.*, 2018, **169**, 132–141.
25 M. Luo, H. Hamdeh and B. H. Davis, Fischer-Tropsch Synthesis: Catalyst activation of low alpha iron catalyst, *Catal. Today*, 2009, **140**(3–4), 127–134.
26 I. O. P. De Berti, J. F. Bengoa, S. J. Stewart, M. V. Cagnoli, G. Pecchi and S. G. Marchetti, Effect of activation atmosphere in the Fischer–Tropsch Synthesis using a "quasi-model" catalyst of γ-Fe2O3 nanoparticles supported on SBA-15, *J. Catal.*, 2016, **335**, 36–46.
27 L. A. Cano, M. V. Cagnoli, J. F. Bengoa, A. M. Alvarez and S. G. Marchetti, Effect of the activation atmosphere on the activity of Fe catalysts supported on SBA-15 in the Fischer–Tropsch Synthesis, *J. Catal.*, 2011, **278**(2), 310–320.
28 J. Xu and C. H. Bartholomew, Temperature-programmed hydrogenation (TPH) and in situ Mössbauer spectroscopy studies of carbonaceous species on silica-supported iron Fischer–Tropsch catalysts, *J. Phys. Chem. B*, 2005, **109**(6), 2392–2403.
29 D. Zhao, Q. Huo, J. Feng, B. F. Chmelka and G. D. Stucky, Nonionic triblock and star diblock copolymer and oligomeric surfactant syntheses of highly ordered, hydrothermally stable, mesoporous silica structures, *J. Am. Chem. Soc.*, 1998, **120**(24), 6024–6036.
30 A. Martínez and C. Lopez, The influence of ZSM-5 zeolite composition and crystal size on the in situ conversion of Fischer–Tropsch products over hybrid catalysts, *Appl. Catal., A*, 2005, **294**(2), 251–259.
31 Z. Ma and M. D. Porosoff, Development of tandem catalysts for CO2 hydrogenation to olefins, *ACS Catal.*, 2019, **9**(3), 2639–2656.
32 H. R. Azizi, A. A. Mirzaei, M. Kaykhaii and M. Mansouri, Fischer–Tropsch synthesis: studies effect of reduction variables on the performance of Fe–Ni–Co catalyst, *J. Nat. Gas Sci. Eng.*, 2014, **18**, 484–491.
33 H. Kölbel and M. Ralek, The Fischer-Tropsch synthesis in the liquid phase, *Catal. Rev.:Sci. Eng.*, 1980, **21**(2), 225–274.
34 S. Marchetti, M. Cagnoli, A. Alvarez, J. Bengoa, R. Mercader and A. Yeramián, Study of the Fe/zeolite-L system: Part I: characterization of iron species and their structural properties, *Appl. Surf. Sci.*, 2000, **165**(2–3), 91–99.
35 R. M. Mohamed, H. M. Aly, M. F. El-Shahat and I. A. Ibrahim, Effect of the silica sources on the crystallinity of nanosized ZSM-5 zeolite, *Microporous Mesoporous Mater.*, 2005, **79**(1–3), 7–12.
36 D. Leshchev, M. Rakitin, B. Luvizotto, R. Kadyrov, B. Ravel, K. Attenkofer and E. Stavitski, The Inner Shell Spectroscopy beamline at NSLS-II: a facility for in situ and operando X-ray absorption spectroscopy for materials research, *J. Synchrotron Radiat.*, 2022, **29**(4), 1095–1106.
37 E. de Smit, F. Cinquini, A. M. Beale, O. V. Safonova, W. van Beek, P. Sautet and B. M. Weckhuysen, Stability and reactivity of ε–χ–θ iron carbide catalyst phases in Fischer–Tropsch synthesis: Controlling μC, *J. Am. Chem. Soc.*, 2010, **132**(42), 14928–14941.
38 C. H. Camp Jr, PyMCR: A python library for multivariatecurve resolution analysis with alternating regression (MCR-AR), *J. Res. Natl. Inst. Stand. Technol.*, 2019, **124**, 1.
39 R. Liu, D. Leshchev, E. Stavitski, M. Juneau, J. N. Agwara and M. D. Porosoff, Selective hydrogenation of CO2 and CO over potassium promoted Co/ZSM-5, *Appl. Catal., B*, 2021, **284**, 119787.
40 J. N. Agwara, N. J. Bakas, M. L. Neidig and M. D. Porosoff, Challenges and Opportunities of Fe-based Core-Shell Catalysts for Fischer-Tropsch Synthesis, *ChemCatChem*, 2022, **14**(19), e202200289.
41 R. Liu, Z. Ma, J. D. Sears, M. Juneau, M. L. Neidig and M. D. Porosoff, Identifying correlations in Fischer-Tropsch synthesis and CO2 hydrogenation over Fe-based ZSM-5 catalysts, *J. CO2 Util.*, 2020, **41**, 101290.
42 W. Chen, Z. Fan, X. Pan and X. Bao, Effect of confinement in carbon nanotubes on the activity of Fischer–Tropsch iron catalyst, *J. Am. Chem. Soc.*, 2008, **130**(29), 9414–9419.
43 J.-Y. Park, Y.-J. Lee, P. K. Khanna, K.-W. Jun, J. W. Bae and Y. H. Kim, Alumina-supported iron oxide nanoparticles as Fischer–Tropsch catalysts: Effect of particle size of iron oxide, *J. Mol. Catal. A: Chem.*, 2010, **323**(1–2), 84–90.
44 W. Jóźwiak, T. Maniecki, A. Basińska, J. Goralski and R. Fiedorow, Reduction requirements for Ru/(K) Fe 2 O 3 catalytic activity in water-gas shift reaction, *Kinet. Catal.*, 2004, **45**, 879–889.
45 J. Chen, Q. Zhao, X. Han, J. Lv, Z. Li, S. Huang and X. Ma, Extremely Low CO/H2 Ratio Activation of a Precipitated Iron Catalyst for Enhanced Fischer–Tropsch Performance, *Energy Fuels*, 2022, **36**(10), 5384–5392.
46 C. H. Bartholomew, Mechanisms of catalyst deactivation, *Appl. Catal., A*, 2001, **212**(1–2), 17–60.
47 E. de Smit and B. M. Weckhuysen, The renaissance of iron-based Fischer–Tropsch synthesis: on the multifaceted catalyst deactivation behaviour, *Chem. Soc. Rev.*, 2008, **37**(12), 2758–2781.
48 M. Romero-Sáez, D. Divakar, A. Aranzabal, J. González-Velasco and J. González-Marcos, Catalytic oxidation of trichloroethylene over Fe-ZSM-5: Influence of the preparation method on the iron species and the catalytic behavior, *Appl. Catal., B*, 2016, **180**, 210–218.
49 M. Pérez-Page, J. Makel, K. Guan, S. Zhang, J. Tringe, R. H. Castro and P. Stroeve, Gas adsorption properties of ZSM-5 zeolites heated to extreme temperatures, *Ceram. Int.*, 2016, **42**(14), 15423–15431.
50 W.-S. Lin, H.-M. Lin, H.-H. Chen, Y.-K. Hwu and Y.-J. Chiou, Shape effects of iron nanowires on hyperthermia treatment, *J. Nanomater.*, 2013, **2013**, 9–9.
51 Y. Sun, P. Gao, Y. Han and D. Ren, Reaction behavior of iron minerals and metallic iron particles growth in coal-based reduction of an oolitic iron ore, *Ind. Eng. Chem. Res.*, 2013, **52**(6), 2323–2329.

52 B. Qu, C. Zhu, C. Li, X. Zhang and Y. Chen, Coupling hollow Fe3O4–Fe nanoparticles with graphene sheets for high-performance electromagnetic wave absorbing material, *ACS Appl. Mater. Interfaces*, 2016, **8**(6), 3730–3735.

53 C. Yang, H. Zhao, Y. Hou and D. Ma, Fe5C2 nanoparticles: a facile bromide-induced synthesis and as an active phase for Fischer–Tropsch synthesis, *J. Am. Chem. Soc.*, 2012, **134**(38), 15814–15821.

54 S. Nikitenko, Y. Koltypin, I. Felner, I. Yeshurun, A. Shames, J. Jiang, V. Markovich, G. Gorodetsky and A. Gedanken, Tailoring the properties of Fe–Fe3C Nanocrystalline particles prepared by sonochemistry, *J. Phys. Chem. B*, 2004, **108**(23), 7620–7626.

55 C. Ma, W. Zhang, Q. Chang, X. Wang, H. Wang, H. Chen, Y. Wei, C. Zhang, H. Xiang and Y. Yang, θ-Fe3C dominated Fe@ C core–shell catalysts for Fischer-Tropsch synthesis: Roles of θ-Fe3C and carbon shell, *J. Catal.*, 2021, **393**, 238–246.

56 T. Herranz, S. Rojas, F. J. Pérez-Alonso, M. Ojeda, P. Terreros and J. L. G. Fierro, Genesis of iron carbides and their role in the synthesis of hydrocarbons from synthesis gas, *J. Catal.*, 2006, **243**(1), 199–211.

57 X. Yang, R. Wang, J. Yang, W. Qian, Y. Zhang, X. Li, Y. Huang, T. Zhang and D. Chen, Exploring the reaction paths in the consecutive Fe-based FT catalyst–zeolite process for syngas conversion, *ACS Catal.*, 2020, **10**(6), 3797–3806.

58 G. Fierro, G. Moretti, G. Ferraris and G. B. Andreozzi, A Mössbauer and structural investigation of Fe-ZSM-5 catalysts: Influence of Fe oxide nanoparticles size on the catalytic behaviour for the NO-SCR by C3H8, *Appl. Catal., B*, 2011, **102**(1–2), 215–223.

59 Z. Ma, H. Ma, H. Zhang, X. Wu, W. Qian, Q. Sun and W. Ying, Direct conversion of syngas to light olefins through Fischer–Tropsch synthesis over Fe–Zr catalysts modified with sodium, *ACS Omega*, 2021, **6**(7), 4968–4976.

60 J. Li, X. Cheng, C. Zhang, J. Wang, W. Dong, Y. Yang and Y. Li, Alkalis in iron-based Fischer–Tropsch synthesis catalysts: distribution, migration and promotion, *J. Chem. Technol. Biotechnol.*, 2017, **92**(6), 1472–1480.

61 Y. Chen, H. Zhang, H. Ma, W. Qian, F. Jin and W. Ying, Direct conversion of syngas to ethanol over Rh–Fe/γ-Al 2 O 3 catalyst: Promotion effect of Li, *Catal. Lett.*, 2018, **148**, 691–698.

62 Z. Han, W. Qian, H. Ma, X. Wu, H. Zhang, Q. Sun and W. Ying, Study of the Fischer–Tropsch synthesis on nano-precipitated iron-based catalysts with different particle sizes, *RSC Adv.*, 2020, **10**(70), 42903–42911.

63 X. Yang, H. Zhang, Y. Liu, W. Ning, W. Han, H. Liu and C. Huo, Preparation of iron carbides formed by iron oxalate carburization for Fischer–Tropsch synthesis, *Catalysts*, 2019, **9**(4), 347.

64 H. Suo, S. Wang, C. Zhang, J. Xu, B. Wu, Y. Yang, H. Xiang and Y.-W. Li, Chemical and structural effects of silica in iron-based Fischer–Tropsch synthesis catalysts, *J. Catal.*, 2012, **286**, 111–123.

65 A. N. Pour, M. R. Housaindokht, S. F. Tayyari, J. Zarkesh and M. R. Alaei, Deactivation studies of Fischer–Tropsch synthesis on nano-structured iron catalyst, *J. Mol. Catal. A: Chem.*, 2010, **330**(1–2), 112–120.

66 J. Xu, C. H. Bartholomew, J. Sudweeks and D. L. Eggett, Design, synthesis, and catalytic properties of silica-supported, Pt-promoted iron Fischer–Tropsch catalysts, *Top. Catal.*, 2003, **26**, 55–71.